



OXFORD CENTRE FOR COLLABORATIVE APPLIED MATHEMATICS

Report Number 10/42

**On the Linear Stability of the Fifth-Order WENO Discretization**

by

**Mohammad Motamed, Colin B. Macdonald, and Steven J. Ruuth**



Oxford Centre for Collaborative Applied Mathematics  
Mathematical Institute  
24 - 29 St Giles'  
Oxford  
OX1 3LB  
England



# On the Linear Stability of the Fifth-Order WENO Discretization

Mohammad Motamed\*      Colin B. Macdonald<sup>†</sup>

Steven J. Ruuth<sup>‡</sup>

August 2, 2010

**Abstract** We study the linear stability of the fifth-order Weighted Essentially Non-Oscillatory spatial discretization (WENO5) combined with explicit time stepping applied to the one-dimensional advection equation. We show that it is not necessary for the stability domain of the time integrator to include a part of the imaginary axis. In particular, we show that the combination of WENO5 with either the forward Euler method or a two-stage, second-order Runge–Kutta method is linearly stable provided very small time step-sizes are taken. We also consider fifth-order multistep time discretizations whose stability domains do not include the imaginary axis. These are found to be linearly stable with moderate time steps when combined with WENO5. In particular, the fifth-order extrapolated BDF scheme gave superior results in practice to high-order Runge–Kutta methods whose stability domain includes the imaginary axis. Numerical tests are presented which confirm the analysis.

**Keywords** linear stability analysis, method of lines, WENO, multistep methods, Runge–Kutta methods, hyperbolic conservation laws

## 1 Introduction

The method of lines is a general technique for solving time-dependent partial differential equations (PDEs). In this approach, the PDEs are first discretized on a

---

\*Department of Mathematics, Simon Fraser University, Burnaby, BC, V5A 1S6, Canada ([mmotamed@math.sfu.ca](mailto:mmotamed@math.sfu.ca)). The work of this author was partially supported by NSERC Canada.

<sup>†</sup>Mathematical Institute, University of Oxford, Oxford, OX1 3LB, UK ([macdonald@maths.ox.ac.uk](mailto:macdonald@maths.ox.ac.uk)). The work of this author was supported by NSERC Canada, NSF grant number CCF-0321917, and by Award No KUK-C1-013-04 made by King Abdullah University of Science and Technology (KAUST).

<sup>‡</sup>Department of Mathematics, Simon Fraser University, Burnaby, BC, V5A 1S6, Canada ([sruuth@sfu.ca](mailto:sruuth@sfu.ca)). The work of this author was partially supported by NSERC Canada.

spatial grid and a system of ordinary differential equations (ODEs) in time is obtained. The approximate solution is then computed by a suitable time integrator.

Hyperbolic conservation laws are a set of PDEs, often nonlinear, whose wave-like solutions may develop discontinuities, even in the presence of smooth initial conditions. When applying the method of lines to problems involving discontinuous solutions, in addition to linear stability, a stronger nonlinear stability is often desirable. Linear stability is required for preventing the numerical solutions from blowing up, and nonlinear stability is needed for resolving discontinuities without generating spurious oscillations. Suitable spatial discretizations include total-variation-diminishing (TVD) schemes [15, 6], total-variation-bounded (TVB) schemes [17], essentially non-oscillatory (ENO) schemes [8, 7, 20], and weighted essentially non-oscillatory (WENO) schemes [14, 10, 19]. These spatial discretizations are often combined with strong stability preserving (SSP) Runge–Kutta and multistep time-stepping schemes. SSP time-stepping schemes preserve convex boundedness and contractivity properties of the spatial discretization combined with forward Euler, under a modified time-step restriction [20, 18, 3, 4, 16, 11].

In this paper, we consider the popular WENO5 method [10]. WENO5 uses a weighted combination of three stencils of the third order ENO scheme with nonlinear weights. WENO5 is therefore a nonlinear spatial discretization. We freeze the nonlinear weights and study the linear stability of the resulting linear finite difference discretization, combined with different types of explicit time-stepping schemes applied to the one-dimensional advection equation. We note that the analysis presented here is also applicable to more general hyperbolic conservation laws with a bounded flux derivative. The linear analysis provides insight into the behavior of the nonlinear WENO5 method applied to nonlinear problems and problems with discontinuous solutions.

The linear stability of WENO5 (in the above frozen-coefficient sense) has been studied in [10, 21]. These studies consider WENO5 in combination with a time-stepping scheme whose linear stability domain includes a part of the imaginary axis  $[-i\beta, i\beta]$  with  $\beta > 0$ , such as the third-order SSP Runge–Kutta scheme of Shu and Osher [20]. Here, we aim to give a more complete picture of the linear stability of WENO5. The main result of this paper is that the inclusion of imaginary axis is not a necessary condition, and that there are time integrators which do not satisfy this condition and yet are suitable to use in combination with WENO5. In particular, we show that the combination of WENO5 with either the forward Euler (FE) method or a two-stage, second-order explicit Runge–Kutta (ERK2) method is linearly stable provided very small time step-sizes are taken. We further show that fifth-order multistep time discretizations whose stability domain does not include the imaginary axis can possess suitable linear stability properties when combined with WENO5. Of these schemes, the extrapolated BDF5 scheme is particularly recommended. It possesses a mild linear stability restriction and performs well in situations where other high-order schemes generate spurious oscillations.

The outline of the paper is as follows. In Section 2, we review the linear stability

analysis for the method of lines applied to the one-dimensional advection equation. In Section 3, we first review the linearization of WENO5 by freezing the nonlinear weights. Then the linear stability of the resulting finite difference scheme is studied in combination with various explicit Runge–Kutta and multistep methods. Numerical tests on both linear and nonlinear problems using the fully nonlinear WENO5 are presented in Section 4 to confirm the analysis.

## 2 Linear Stability Analysis

We consider the one-dimensional scalar advection equation

$$u_t + u_x = 0, \quad x \in [0, 1], \quad t > 0, \quad (1)$$

with periodic boundary conditions and initial conditions

$$u(x, t = 0) = u^0(x), \quad x \in [0, 1]. \quad (2)$$

We study the linear stability of approximate solutions of (1) when the method of lines is employed. In this approach, we first discretize the PDE on a uniform spatial grid and obtain a system of ODEs in time. We then compute the approximate solution by an explicit Runge–Kutta (ERK) or an explicit linear multistep (ELM) time integrator.

Let  $\Delta x = \frac{1}{N}$  denote the spatial grid-length, where  $N$  is a natural number. Without loss of generality, we assume  $N$  is an even number. For  $j = 0, 1, \dots, N$ , let  $x_j = j \Delta x$  and  $u_j(t)$  denote the corresponding grid point and the grid function approximating  $u(x_j, t)$ , respectively. On this spatial grid, we discretize (1) by a finite difference scheme to obtain the semi-discretization,

$$\frac{d}{dt} u_j(t) = \frac{-1}{\Delta x} L(u_{j-r}, \dots, u_{j+s}). \quad (3)$$

We now briefly review the type of linear stability analysis that we use in this paper.

### 2.1 von Neumann Analysis

von Neumann analysis is one of the most popular types of linear stability analysis, see for example [9, 12]. It applies to linear systems of equations with periodic boundary conditions. In this technique, the semi-discrete solution is expressed by a discrete Fourier series in space,

$$u_j(t) = \sum_{m=-N/2}^{N/2} \hat{u}_m(t) e^{i\omega_m j \Delta x}, \quad \omega_m \in \mathbb{R}.$$

By the superposition principle, we can use only one term in the series

$$u_j(t) = \hat{u}_m(t) e^{ij\theta_m}, \quad \theta_m = \omega_m \Delta x, \quad (4)$$

where  $m = -N/2, \dots, N/2$ .

In order to use von Neumann analysis, we assume that the operator  $L$  in (3) can be written in the form

$$L(u_{j-r}, \dots, u_{j+s}) = z(\theta_m) u_j. \quad (5)$$

Here the complex function  $z$  is called the Fourier symbol of the spatial operator  $L$ . For example, if  $L$  is a linear operator, it can be written in the form (5). As we will see in the next section, the operator for WENO5 can be approximated by a linear operator in this form when the solution is smooth.

Now let the semi-discrete system (3) and (5) be discretized by an explicit time integrator with a time step-size  $\Delta t$ . Let  $u_j^n = u_j(t^n)$  denote the solution at the  $n$ -th time level  $t^n = n \Delta t$ . By inserting (4) into the resulting fully-discrete system, we can write

$$u_j^{n+1} = g(\hat{z}_m) u_j^n, \quad \hat{z}_m = -\sigma z(\theta_m), \quad m = -N/2, \dots, N/2, \quad n \geq 1, \quad (6)$$

where the *amplification factor*  $g$  is a function of  $\theta_m$  and the *CFL number*  $\sigma = \frac{\Delta t}{\Delta x}$ . The amplification factor is a property of the time-stepping scheme.

In standard von Neumann analysis, as a simplification, we drop the subscript  $m$  and obtain

$$u_j^{n+1} = g(\hat{z}) u_j^n, \quad \hat{z} = -\sigma z(\theta), \quad (7)$$

where  $g$  is now a function of  $\theta$  and  $\sigma$ . The dependencies on  $m$  and  $N$  have thus been eliminated. This simplification is equivalent to taking the limit  $N \rightarrow \infty$  and considering a continuous function  $\theta$  instead of a discrete set  $\theta_m$  with  $m = -N/2, \dots, N/2$ .

A spatial discretization method combined with an explicit temporal discretization is linearly stable if the amplification factor satisfies the condition

$$|g(-\sigma z(\theta))| \leq 1, \quad \forall \theta \in [0, 2\pi]. \quad (8)$$

This stability condition imposes an upper bound on  $\sigma$  which in turn enables us to find a time step-size for which the method is linearly stable. The largest possible number  $\sigma > 0$  which satisfies this condition is denoted by  $\sigma_a$  and we call it the *algebraic stability limit* for the particular spatial discretization and time-stepping scheme. We note that this condition is not necessary for the usual definition of stability: the right hand side can be relaxed to  $1 + C \Delta t$ . Here, we consider the so called ‘‘absolute stability’’ which guarantees a stronger bound than the usual stability (resulting in long time boundedness of the numerical solution).

Our usage of the term *algebraic* above is intended to be in contrast the following geometric approach (specifically, it is independent of the concept of algebraic stability of Runge–Kutta methods [5]). We now give a geometrical interpretation of the linear stability [1, 13, 21]. We start with the following definitions.

**Definition 1** The spectrum of a spatial discretization scheme (3) and (5) with  $N \rightarrow \infty$  is the set  $\mathcal{S} = \{-z(\theta) : 0 \leq \theta \leq 2\pi\}$ .

**Definition 2** The linear stability domain of an explicit time-stepping scheme with amplification factor  $g(\hat{z})$  is  $\mathcal{S}_t = \{\hat{z} : |g(\hat{z})| \leq 1\}$ .

**Definition 3** The geometric stability limit, denoted by  $\sigma_g$ , is the largest number  $\tilde{\sigma}$  such that the rescaled spectrum  $\tilde{\sigma} \mathcal{S}$  lies inside the linear stability domain  $\mathcal{S}_t$ ,

$$\tilde{\sigma} \mathcal{S} \subseteq \mathcal{S}_t. \quad (9)$$

We will refer to this condition as *geometric stability condition*. Note that either approach gives the same results, and thus the algebraic and geometric stability limits are equal,  $\sigma_g = \sigma_a$ .

**Example.** The operator  $L$  for upwind spatial discretization reads

$$L(u_{j-1}, u_j) = u_j - u_{j-1},$$

and can be written in the form (5) with  $z(\theta) = 1 - e^{-i\theta}$ . The corresponding spectrum  $\mathcal{S}$  is therefore a circle of radius 1 centered at  $(-1, 0)$  in the complex plane. Now if we use FE time discretization with  $g(\hat{z}) = 1 + \hat{z}$ , the stability domain  $\mathcal{S}_t$  is a disc whose boundary is precisely the same as  $\mathcal{S}$ , and we have  $\sigma_g = 1$ . Moreover, it is trivial that  $\sigma_a = 1$ . Therefore we have  $\sigma_g = \sigma_a = 1$ .

In the next section, using the geometrical interpretation of linear stability, we will show that problems may arise when applying the standard von Neumann analysis. We then present a modification to the standard von Neumann analysis in order to overcome such problems.

## 2.2 Modified von Neumann Analysis

The last step in the standard von Neumann analysis is the simplification step which replaces the discrete set of  $N+1$  phases  $\theta_m$ ,  $m = -N/2, \dots, N/2$ , with a continuous phase function  $\theta \in [0, 2\pi]$ . This simplification step may cause a problem for certain spatial and temporal discretizations. We begin by illustrating the problem with a particular example. We then show how to modify the analysis to resolve such problems.

To illustrate the main idea, suppose that the continuous spectrum  $\mathcal{S}$  corresponding to a (fictitious) spatial discretization of the advection equation takes the form of a cubic curve in a neighborhood of the origin in the complex plane, with

$$\operatorname{Re}(z) = \theta^3, \quad \operatorname{Im}(z) = -\theta, \quad 0 \leq \theta \ll 1.$$

Furthermore, suppose FE time discretization is used. The boundary of the linear stability domain  $\partial\mathcal{S}_t$  is a circle of radius 1 centered at  $(-1, 0)$  in the complex plane.

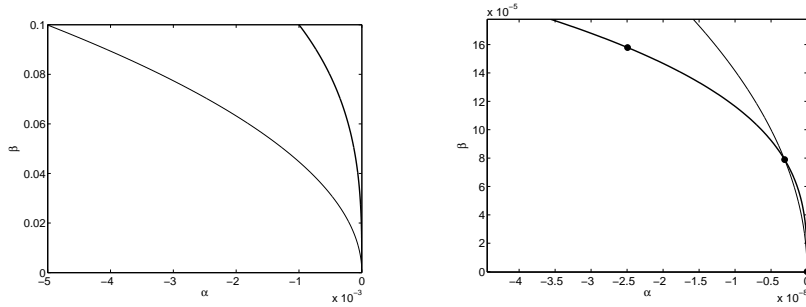


Figure 1: The left figure shows the spectrum  $\mathcal{S}$  of a fictitious spatial discretization (thick-line) which takes the form of a cubic curve and the boundary of the stability domain  $\partial\mathcal{S}_t$  of FE time stepping (thin-line) in a neighborhood of the origin in the complex plane. The right figure shows the first two eigenvalues close to origin multiplied by a nonzero stability limit,  $-\sigma_g z(\Delta\theta)$  and  $-\sigma_g z(2\Delta\theta)$ .

See Figure 1 (left). According to the geometric stability condition (9), we need to rescale the spectrum  $\mathcal{S}$  (thick-line) by  $\sigma_g$  such that it lies inside the FE stability domain with the boundary  $\partial\mathcal{S}_t$  (thin-line). The geometric stability condition (9) can be expressed as

$$(1 - \tilde{\sigma} \operatorname{Re}(z))^2 + (\tilde{\sigma} \operatorname{Im}(z))^2 \leq 1,$$

which gives

$$\sigma_g = \frac{2\theta}{1 - \theta^4}, \quad 0 < \theta \ll 1. \quad (10)$$

Note that for the particular case  $\theta = 0$ ,  $\sigma_g \mathcal{S}$  lies on  $\partial\mathcal{S}_t$ . This relation shows that in the limit as  $\theta \rightarrow 0$  we obtain  $\sigma_g = 0$  which implies that we need a zero CFL number. This result is too strict, however, since we only need to fit the eigenvalues on the spectrum corresponding to the  $N + 1$  phases  $\theta_m$ ,  $m = -N/2, \dots, N/2$ . This observation leads us to introduce the discrete spectrum.

**Definition 4** The discrete spectrum  $\mathbf{S}$  of a spatial discretization scheme (3) and (5) is the set of  $N + 1$  eigenvalues  $\mathbf{S} = \{-z(\theta_m) : \theta_m \in \{0, \Delta\theta, 2\Delta\theta, \dots, 2\pi\}, \Delta\theta = 2\pi\Delta x\}$ .

The *discrete geometric stability condition* now reads

$$\tilde{\sigma} \mathbf{S} \subseteq \mathcal{S}_t, \quad (11)$$

where  $\tilde{\sigma}$  and the geometric stability limit  $\sigma_g$  are henceforth defined correspondingly.

We now apply this condition to the example in this section. In a neighborhood of the origin, the linear stability restriction is determined by the nonzero eigenvalue



that is closest to the origin,  $-z(\Delta\theta)$ . Using this eigenvalue and equation (10), we obtain the following time-step restriction for FE,

$$\sigma_g = \frac{4\pi\Delta x}{1 - 16\pi^4\Delta x^4} \quad \Rightarrow \quad \Delta t \leq \frac{4\pi\Delta x^2}{1 - 16\pi^4\Delta x^4}.$$

Using this stability limit, we can fit the discrete linear stability domain inside the linear stability domain of FE. See Figure 1 (right) for the corresponding plot near the origin.

Note however that checking the behaviour of eigenvalues near the origin is not sufficient: condition (11) must be satisfied for all of  $\mathbf{S}$ . In our calculations, this check is carried out using a straightforward examination of the plots and a simple bisection search.

Throughout this paper, linear stability is assessed using this modified von Neumann analysis rather than the standard von Neumann analysis. This allows us to obtain sharp bounds on time-stepping restrictions. In several cases, modified von Neumann analysis allows us to report finite stability restrictions when the standard von Neumann analysis would have indicated instability.

### 3 WENO5 Method

In this section, we study the linear stability properties of a finite difference scheme obtained by “freezing” the nonlinear weights of the WENO5 spatial discretization. We first calculate the stability region of this “linearized WENO5” scheme. We then consider different time-stepping schemes and obtain proper geometric stability limits such that their combination with linearized WENO5 is linearly stable. Note that our numerical results in Section 4 demonstrate that this analysis of the linearized WENO5 scheme is consistent with what we observe in practice with the full nonlinear WENO5 method.

#### 3.1 WENO5 Spatial Discretization

The operator  $L$  in (3) for WENO5 reads

$$L(u_{j-3}, \dots, u_{j+2}) = \hat{f}_{j+1/2} - \hat{f}_{j-1/2}, \quad (12)$$

where  $\hat{f}_{j+1/2}$  is the numerical flux. In the case of linear advection, it is given by

$$\begin{aligned} \hat{f}_{j+1/2} = w_0 \left( \frac{2}{6}u_{j-2} - \frac{7}{6}u_{j-1} + \frac{11}{6}u_j \right) + w_1 \left( -\frac{1}{6}u_{j-1} + \frac{5}{6}u_j + \frac{2}{6}u_{j+1} \right) + \\ + w_2 \left( \frac{2}{6}u_j + \frac{5}{6}u_{j+1} - \frac{1}{6}u_{j+2} \right). \end{aligned}$$

The weights  $w_{0,1,2}$  are computed based on the smoothness indicators [10]

$$\begin{aligned} IS_0 &= \frac{13}{12}(u_{j-2} - 2u_{j-1} + u_j)^2 + \frac{1}{4}(u_{j-2} - 4u_{j-1} + 3u_j)^2, \\ IS_1 &= \frac{13}{12}(u_{j-1} - 2u_j + u_{j+1})^2 + \frac{1}{4}(u_{j-1} - u_{j+1})^2, \\ IS_2 &= \frac{13}{12}(u_j - 2u_{j+1} + u_{j+2})^2 + \frac{1}{4}(3u_j - 4u_{j+1} + u_{j+2})^2. \end{aligned}$$

The weights are given by

$$w_l = \frac{\alpha_l}{\sum_{k=0}^2 \alpha_k}, \quad \alpha_l = \frac{d_l}{(\epsilon + IS_l)^2}, \quad l = 0, 1, 2,$$

where  $d_0 = \frac{1}{10}$ ,  $d_1 = \frac{6}{10}$ ,  $d_2 = \frac{3}{10}$ , and  $\epsilon$  is a small number typically introduced to avoid singularity.

### 3.2 Linearization of WENO5

In regions where the solution is smooth, Taylor expansion of the smoothness indicators gives

$$IS_l = \frac{13}{12}((\Delta x)^2 u_j'')^2 + \frac{1}{4}(2\Delta x u_j' + c_l(\Delta x)^3 u_j''')^2 + \mathcal{O}((\Delta x)^6), \quad l = 0, 1, 2,$$

where  $c_0 = \frac{-2}{3}$ ,  $c_1 = \frac{1}{3}$ ,  $c_2 = \frac{-2}{3}$ ,  $u_j' = u_x(x_j, t)$ ,  $u_j'' = u_{xx}(x_j, t)$  and  $u_j''' = u_{xxx}(x_j, t)$ . We therefore have

$$IS_l = C(1 + \mathcal{O}((\Delta x)^2)), \quad l = 0, 1, 2.$$

If  $u_j' \neq 0$ , then  $C = (\Delta x u_j')^2$ , and if  $u_j' = 0$ , then  $C = \frac{13}{12}((\Delta x)^2 u_j'')^2$  [10]. Therefore,  $C$  is a nonzero quantity and independent of  $l$ . As a result of this, we can show

$$w_l = d_l + \delta_l, \quad \delta_l = \mathcal{O}((\Delta x)^2), \quad \sum_{k=0}^2 \delta_k = 0, \quad l = 0, 1, 2. \quad (13)$$

For example in the case  $1/u_j' = \mathcal{O}(1)$ , we have

$$\delta_l = b_l \frac{u_j'''}{u_j'} (\Delta x)^2 + \mathcal{O}((\Delta x)^4), \quad b_0 = \frac{3}{25}, \quad b_1 = \frac{-12}{25}, \quad b_2 = \frac{9}{25}.$$

Neglecting the small terms  $\delta_l$ , we obtain

$$\hat{f}_{j+1/2} = \frac{2}{60}u_{j-2} - \frac{13}{60}u_{j-1} + \frac{47}{60}u_j + \frac{27}{60}u_{j+1} - \frac{3}{60}u_{j+2},$$

and the operator  $L$  is

$$L = -\frac{2}{60}u_{j-3} + \frac{15}{60}u_{j-2} - \frac{60}{60}u_{j-1} + \frac{20}{60}u_j + \frac{30}{60}u_{j+1} - \frac{3}{60}u_{j+2}.$$

Considering solutions of type (4), we get

$$z(\theta_m) = \frac{16}{15} \sin^6 \frac{\theta_m}{2} + i \left( -\frac{1}{6} \sin 2\theta_m + \frac{4}{3} \sin \theta_m + \frac{16}{15} \sin^5 \frac{\theta_m}{2} \cos \frac{\theta_m}{2} \right).$$

Since the eigenvalues  $-z(\theta_m)$  sit on the spectrum  $\mathbf{S}$  in a clock-wise order as  $\theta_m$  increases from 0 to  $2\pi$ , in order to be consistent with the standard polar form of numbers in the complex plane, which have a counter clock-wise order in  $\theta_m$ , we replace  $\theta_m$  by  $2\pi - \theta_m$  and write

$$z_m := z(\theta_m) = \frac{16}{15} \sin^6 \frac{\theta_m}{2} + i \left( \frac{1}{6} \sin 2\theta_m - \frac{4}{3} \sin \theta_m - \frac{16}{15} \sin^5 \frac{\theta_m}{2} \cos \frac{\theta_m}{2} \right). \quad (14)$$

The corresponding spectrum is obtained by multiplying (14) by  $-1$  and is shown in Figure 2.

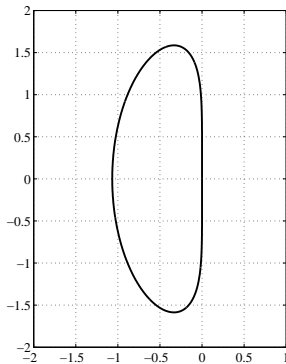


Figure 2: The spectrum  $\mathbf{S}$  of the finite difference scheme resulting from linearizing WENO5 in smooth regions.

Note that, as the above formula suggests, for small values of  $\theta_m$  and  $2\pi - \theta_m$ , the eigenvalues lie very close to the imaginary axis. This is the main reason that a time discretization whose linear stability domain  $\mathcal{S}_t$  includes a part of imaginary axis  $[-i\beta, i\beta]$  with  $\beta > 0$  has been considered in [10, 21]. This will then ensure that (11) holds for some  $\bar{\sigma} > 0$ . However, as we will show in this section, the inclusion of the imaginary axis is not a necessary condition, and there are many time integrators which do not satisfy this condition and yet are suitable to be combined with WENO5.

It is particularly important to study the spectrum in a neighborhood of the origin where  $\theta_m$  values are small. This can be done analytically using Taylor expansions of the function  $z(\theta)$  around  $\theta = 0$  [21]. Thus, in order to find the largest  $\tilde{\sigma}$  such that (11) holds for a particular time-stepping scheme, we first analytically study the spectrum of linearized WENO5 in a neighborhood of the origin and find a scale  $\sigma_g$  such that the rescaled spectrum  $\sigma_g \mathbf{S}$  is contained in  $\mathcal{S}_t$ . Then, by a simple bisection search algorithm, we find a possibly new  $\sigma_g$  for the remaining eigenvalues (apart from the origin). Finally, we select the minimum of the two obtained values as the geometric stability limit for the particular time-stepping scheme.

To carry out our analysis, we will need to approximate  $\mathbf{S}$  near the origin. Using the Taylor expansion, the function (14) in a neighborhood of the origin for small values  $0 < \theta_m \ll 1$  reads

$$\operatorname{Re}(z_m) = \frac{1}{60}\theta_m^6 + \mathcal{O}(\theta_m^8), \quad \operatorname{Im}(z_m) = -\theta_m + \mathcal{O}(\theta_m^7). \quad (15)$$

**Remark 1** The neglect of the small terms  $\delta_l$  in (13) near the origin is only for simplification. If we include these terms, instead of (15) we obtain (as in [21])

$$\operatorname{Re}(z_m) = \frac{7}{60}\theta_m^6 + \mathcal{O}(\theta_m^8), \quad \operatorname{Im}(z_m) = -\theta_m + \mathcal{O}(\theta_m^7).$$

This shows that near the origin, the actual spectrum lies farther from the imaginary axis than what we consider in (15). Therefore, the simplification of neglecting the  $\delta_l$  in our linearization of WENO5 may give stricter-than-necessary stability bounds for the WENO5 scheme.

### 3.3 Temporal Discretizations

We now consider a variety of time discretizations from the class of ERK and ELM methods and study their linear stability when combined with linearized WENO5. A focus of our studies is methods whose stability domain does not include a part of the imaginary axis.

We discretize the semi-discrete system (3) and (5) by either an  $s$ -stage, order- $p$  ERK method, or a  $k$ -step ELM method. An  $s$ -stage, order- $p$  ERK method applied to the semi-discrete system can be written as (7) with the amplification factor [2]

$$g(\hat{z}) = 1 + \sum_{l=1}^p \frac{\hat{z}^l}{l!} + \sum_{l=p+1}^s \hat{z}^l b^\top A^{l-1} \mathbf{1}. \quad (16)$$

Here the elements of matrix  $A \in \mathbb{R}^{s \times s}$  and vector  $b \in \mathbb{R}^s$  are the coefficients of the Butcher tableau, and  $\mathbf{1} = (1, \dots, 1)^\top$ . Note that  $u_j^0$  is given by the initial data (2).

A general  $k$ -step ELM method for (3) and (5) has the form (e.g., [5])

$$u_j^{n+1} = \sum_{l=1}^k (a_l + b_l \hat{z}) u_j^{n-l+1}, \quad \hat{z} = -\sigma z(\theta), \quad n \geq k \geq 1. \quad (17)$$

Here  $u_j^0$  is given by the initial data (2), and the other  $k - 1$  starting vectors  $u_j^1, \dots, u_j^{k-1}$  are either given or computed by an appropriate starting procedure. We note that since  $u_j^n = (g(\hat{z}))^l u_j^{n-l}$ ,  $0 \leq l \leq n$ , the amplification factor for ELM methods is implicitly given by

$$\hat{z} = \frac{(g(\hat{z}))^k - \sum_{l=1}^k a_l (g(\hat{z}))^{k-l}}{\sum_{l=1}^k b_l (g(\hat{z}))^{k-l}}. \quad (18)$$

### 3.3.1 Forward Euler Method

We start with the FE method and show that there exists a geometric stability limit  $\sigma_g > 0$  such that the combination is linearly stable, albeit for impractically small time steps. FE can be seen both as a one-stage, order-one ERK method and as a one-step, first order ELM method. The amplification factor for FE is  $g(\hat{z}) = 1 + \hat{z}$ , and therefore its stability domain is a disc with radius one and centered at  $(-1, 0)$  in the complex plane. Figure 3 shows the boundary of the stability domain  $\partial\mathcal{S}_t$  of FE together with the spectrum  $\mathbf{S}$  of linearized WENO5.

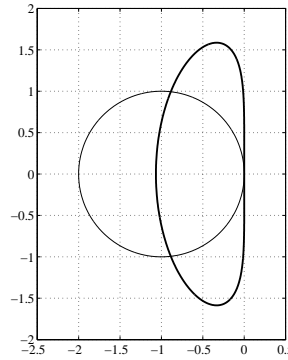


Figure 3: The discrete spectrum  $\mathbf{S}$  of linearized WENO5 in smooth regions (thick-line) and the boundary of the stability domain  $\partial\mathcal{S}_t$  of forward Euler (thin-line).

In this case, the geometric stability condition (11) can be expressed as

$$(1 - \tilde{\sigma} \operatorname{Re}(z_m))^2 + (\tilde{\sigma} \operatorname{Im}(z_m))^2 \leq 1,$$

with  $z_m$  given in (14). After some algebraic manipulation, we obtain for  $\theta_m \neq 0$ ,

$$\begin{aligned} 0 < \sigma_g &= \frac{2\operatorname{Re}(z_m)}{(\operatorname{Re}(z_m))^2 + (\operatorname{Im}(z_m))^2} \\ &= \frac{120 \sin^4 \frac{\theta_m}{2}}{-96 \cos^8 \frac{\theta_m}{2} + 564 \cos^6 \frac{\theta_m}{2} - 1076 \cos^4 \frac{\theta_m}{2} + 769 \cos^2 \frac{\theta_m}{2} + 64}. \end{aligned}$$

This shows that the combination of linearized WENO5 and FE is stable provided the above condition is satisfied. For small values  $0 < \theta_m \ll 1$ , by Taylor expansion we have

$$\sigma_g = \frac{1}{30}\theta_m^4 + \mathcal{O}(\theta_m^6).$$

For the closest eigenvalue to the origin,  $-z(\Delta\theta)$ , we obtain the following time-step restriction for FE,

$$\sigma_g = \frac{(2\pi)^4}{30} \Delta x^4 \quad \Rightarrow \quad \Delta t \leq \frac{8\pi^4}{15} \Delta x^5 \approx 51.95 \Delta x^5.$$

Satisfying this restriction requires prohibitively small time steps, which makes the combination of linearized WENO5 and FE impractical. This is also true of the (fully nonlinear) WENO5 and FE combination as confirmed in Section 4.1.1. Nonetheless, this result demonstrates an important principle, specifically that imaginary axis inclusion is not a necessary property for achieving linear stability. This fact will prove useful when we consider time-stepping schemes whose order matches that of the underlying spatial discretization.

### 3.3.2 Second-order Runge–Kutta Method

We now consider the family of ERK2 methods with the amplification factor given by (16) with  $s = p = 2$ ,

$$g(\hat{z}) = 1 + \hat{z} + \frac{\hat{z}^2}{2}.$$

The boundary of the stability domain,  $\partial\mathcal{S}_t = \{\hat{z} : |g(\hat{z})| = 1\}$ , can be obtained by setting  $g(\hat{z}) = e^{i\phi}$ , with  $\phi \in [0, 2\pi]$ , and solving the second-order algebraic equation,

$$\hat{z}^2 + 2\hat{z} + 2 - 2e^{i\phi} = 0. \quad (19)$$

The spectrum  $\mathbf{S}$  of linearized WENO5 and  $\partial\mathcal{S}_t$  of ERK2 are shown in Figure 4.

After some algebraic manipulation of (19), and using the Taylor expansion for small values of  $0 < \phi \ll 1$  in a neighborhood of the origin we obtain

$$\operatorname{Re}(\hat{z}) = -\frac{1}{8}\phi^4 + \mathcal{O}(\phi^6), \quad \operatorname{Im}(\hat{z}) = \phi - \frac{1}{6}\phi^3 + \mathcal{O}(\phi^5).$$

This implies that  $\partial\mathcal{S}_t$  can be approximated around the origin by the curve

$$\operatorname{Re}(\hat{z}) \approx -\frac{1}{8}(\operatorname{Im}(\hat{z}))^4.$$

Setting  $\operatorname{Im}(\hat{z}) = -\tilde{\sigma}\operatorname{Im}(z_m) \approx \tilde{\sigma}\theta_m$  in (15) we find that in a neighborhood of the origin the condition (11) is satisfied if  $\operatorname{Re}(\hat{z}) \geq -\tilde{\sigma}\operatorname{Re}(z_m)$ . In fact, this condition

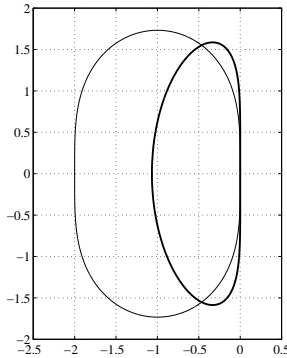


Figure 4: The discrete spectrum  $\mathbf{S}$  of linearized WENO5 in smooth regions (thick-line) and the boundary of the stability domain  $\partial\mathcal{S}_t$  of second order ERK (thin-line).

ensures that for small values of  $\theta_m$  the rescaled spectrum  $\tilde{\sigma} \mathbf{S}$  lie strictly to the left side of the boundary of the linear stability domain  $\partial\mathcal{S}_t$ . Thus

$$-\frac{1}{8}(\tilde{\sigma} \theta_m)^4 \geq -\frac{1}{60} \tilde{\sigma} \theta_m^6 \quad \Rightarrow \quad \sigma_g = \left(\frac{2}{15}\right)^{1/3} \theta_m^{2/3}.$$

As before, the time-stepping restriction arises from the first nonzero eigenvalue of the discrete linearized WENO5 spectrum closest to the origin. Using Taylor series, we obtain the time-step restriction for ERK2,

$$\Delta t \leq \left(\frac{8\pi^2}{15}\right)^{1/3} \Delta x^{5/3} \approx 1.73 \Delta x^{5/3}.$$

This shows that the combination of WENO5 and any ERK2 scheme may not be practical, since very small time steps are required.

### 3.3.3 Five-step, Fifth-order Multistep Methods

In this section we study two popular five-step, fifth-order ELM methods (17) [5]. The first one is the fifth-order explicit Adams method (Adams5), and the second one is the fifth-order extrapolated backward differentiation formula (eBDF5). The coefficients of these two schemes are given in Table 1.

By (18) and setting  $g(\hat{z}) = e^{i\phi}$ , with  $\phi \in [0, 2\pi]$ , the root locus [5], which includes the boundary of stability domain  $\partial\mathcal{S}_t$ , is explicitly given by

$$\hat{z} = \frac{e^{5i\phi} - a_1 e^{4i\phi} - a_2 e^{3i\phi} - a_3 e^{2i\phi} - a_4 e^{i\phi} - a_5}{b_1 e^{4i\phi} + b_2 e^{3i\phi} + b_3 e^{2i\phi} + b_4 e^{i\phi} + b_5}.$$

Table 1: The coefficients in form (17) of two five-step, fifth-order linear multistep schemes.

m	Adams5		eBDF5	
	$a_m$	$b_m$	$a_m$	$b_m$
1	1	1901/720	300/137	300/137
2	0	-2774/720	-300/137	-600/137
3	0	2616/720	200/137	600/137
4	0	-1274/720	-75/137	-300/137
5	0	251/720	12/137	60/137

Figure 5 shows the boundary of the stability domains  $\partial\mathcal{S}_t$  of Adams5 and eBDF5.

Using the Taylor expansion around  $\phi = 0$ , we obtain

$$\operatorname{Re}(\hat{z}) = -\gamma\phi^6 + \mathcal{O}(\phi^8), \quad \operatorname{Im}(\hat{z}) = \phi + \mathcal{O}(\phi^7), \quad (20)$$

in a neighborhood of the origin where  $\gamma = 95/288$  for Adams5 and  $\gamma = 5/6$  for eBDF5. Therefore  $\partial\mathcal{S}_t$  can be approximated near the origin by the curve

$$\operatorname{Re}(\hat{z}) \approx -\gamma(\operatorname{Im}(\hat{z}))^6.$$

Now by (15) and setting  $\operatorname{Im}(\hat{z}) = -\tilde{\sigma}\operatorname{Im}(z_m) \approx \tilde{\sigma}\theta_m$ , the condition (11) is satisfied in a neighborhood of the origin if  $\operatorname{Re}(\hat{z}) \geq -\tilde{\sigma}\operatorname{Re}(z_m)$ . Then

$$-\gamma(\tilde{\sigma}\theta_m)^6 \geq -\frac{1}{60}\tilde{\sigma}\theta_m^6 \quad \Rightarrow \quad \sigma_g = \left(\frac{1}{60\gamma}\right)^{1/5},$$

which gives  $\sigma_g = 0.5504$  and  $\sigma_g = 0.4573$  for Adams5 and eBDF5, respectively. These geometric stability limits are adequate for those eigenvalues on the spectrum  $\mathbf{S}$  which are close to origin. A simple numerical computation shows that in order to fit all eigenvalues into the stability domain  $\mathcal{S}_t$ , we need to take  $\sigma_g = 0.123$  and  $\sigma_g = 0.238$  for Adams5 and eBDF5, respectively. See Figure 5.

### 3.3.4 A Fifth-order Predictor-Corrector Method

In this section we study a fifth-order predictor-corrector [5] time-stepping method (PC5). We first apply the four-step, fourth-order explicit Adams method (the predictor) to (3) using (5). This yields

$$\tilde{u}_j^{n+1} = u_j^n + \hat{z} \left( \frac{55}{24}u_j^n - \frac{59}{24}u_j^{n-1} + \frac{37}{24}u_j^{n-2} - \frac{9}{24}u_j^{n-3} \right).$$

We then use the four-step, fifth-order implicit Adams method as the corrector,

$$u_j^{n+1} = u_j^n + \hat{z} \left( \frac{251}{720}\tilde{u}_j^{n+1} + \frac{646}{720}u_j^n - \frac{264}{720}u_j^{n-1} + \frac{106}{720}u_j^{n-2} - \frac{19}{720}u_j^{n-3} \right).$$



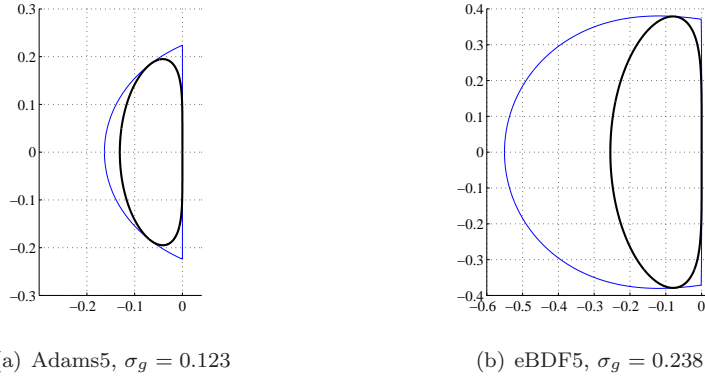


Figure 5: The rescaled discrete spectrum  $\sigma_g \mathbf{S}$  of linearized WENO5 in smooth regions (thick-line) and the boundary of the stability domain  $\partial \mathcal{S}_t$  of Adams5 (left figure, thin-line) and eBDF5 (right figure, thin-line).

It can then be shown that the root locus of PC5 is obtained by solving the second order algebraic equation,

$$\left( \frac{13805}{17280}g^3 - \frac{14809}{17280}g^2 + \frac{9287}{17280}g - \frac{2259}{17280} \right) \hat{z}^2 + \left( \frac{897}{720}g^3 - \frac{264}{720}g^2 + \frac{106}{720}g - \frac{19}{720} \right) \hat{z} + g^3 - g^4 = 0,$$

where  $g = e^{i\phi}$ , with  $\phi \in [0, 2\pi]$ .

Using the Taylor expansion around  $\phi = 0$ , we obtain (20) with  $\gamma = 53281/518400$  in a neighborhood of the origin. Therefore, choosing  $\sigma_g = 0.6950$ , the eigenvalues close to the origin of the rescaled discrete spectrum  $\sigma_g \mathbf{S}$  lie inside the stability domain  $\mathcal{S}_t$  of PC5. A simple numerical computation shows that in order to fit all the eigenvalues into the stability domain  $\mathcal{S}_t$ , we need to take  $\sigma_g = 0.565$ . See Figure 6.

### 3.3.5 High-order Explicit Runge–Kutta Methods

In this section we consider two different high-order Runge–Kutta methods whose linear stability domains include a part of imaginary axis: the three-stage, order-three SSP Runge–Kutta scheme (SSPRK(3,3)) [4] with

$$A = \begin{bmatrix} 0 & 0 & 0 \\ 1 & 0 & 0 \\ \frac{1}{4} & \frac{1}{4} & 0 \end{bmatrix}, \quad b = \begin{bmatrix} \frac{1}{6} \\ \frac{1}{6} \\ \frac{2}{3} \end{bmatrix},$$

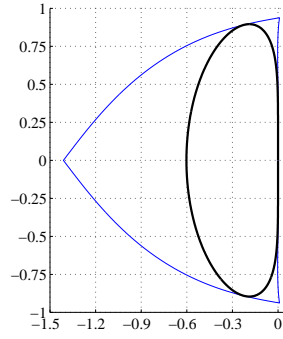
(a)  $\sigma_g = 0.565$ 

Figure 6: The rescaled discrete spectrum  $\sigma_g \mathbf{S}$  of linearized WENO5 in smooth regions (thick-line) and the boundary of the stability domain  $\partial \mathcal{S}_t$  of PC5 (thin-line).

and the seven-stage, order-five Dormand–Prince scheme (DP5) [2, 5] with

$$A = \begin{bmatrix} 0 & 0 & 0 & 0 & 0 & 0 & 0 \\ \frac{1}{5} & 0 & 0 & 0 & 0 & 0 & 0 \\ \frac{3}{40} & \frac{9}{40} & 0 & 0 & 0 & 0 & 0 \\ \frac{44}{45} & -\frac{56}{15} & \frac{32}{9} & 0 & 0 & 0 & 0 \\ \frac{19372}{6561} & -\frac{25360}{2187} & \frac{64448}{6561} & -\frac{212}{729} & 0 & 0 & 0 \\ \frac{9017}{3168} & -\frac{355}{33} & \frac{46732}{5247} & \frac{49}{176} & -\frac{5103}{18656} & 0 & 0 \\ \frac{35}{384} & 0 & \frac{500}{1113} & \frac{125}{192} & -\frac{2187}{6784} & \frac{11}{84} & 0 \end{bmatrix}, \quad b = \begin{bmatrix} \frac{35}{384} \\ 0 \\ \frac{500}{1113} \\ \frac{125}{192} \\ -\frac{2187}{6784} \\ \frac{11}{84} \\ 0 \end{bmatrix}.$$

These methods require three and six function evaluations at each time step, respectively. We note that, despite the fact that the DP5 method has seven stages, it uses only six function evaluations per step because the last stage is evaluated at the same point as the first stage of the next step (the “FSAL” or first-stage-as-last property [5]). Figure 7 shows the rescaled discrete spectrum  $\sigma_g \mathbf{S}$  of linearized WENO5 and the boundary of the stability domains  $\partial \mathcal{S}_t$  of these two Runge–Kutta methods. We will use these Runge–Kutta methods in numerical computations as a comparison with methods which do not include a part of the imaginary axis.

In Table 2, we summarize the linear stability time-step restrictions and the number of function evaluations per time step for all the time-stepping schemes considered in this paper.

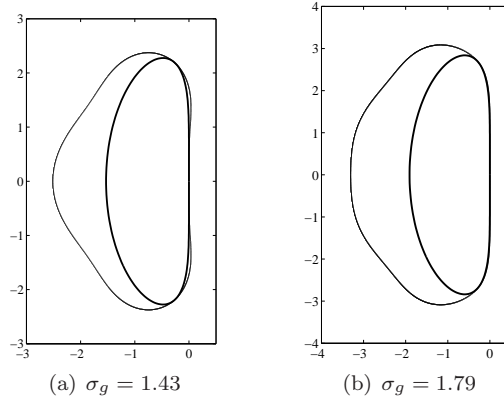


Figure 7: The rescaled discrete spectrum  $\sigma_g \mathbf{S}$  of linearized WENO5 in smooth regions (thick-line) and the boundary of the stability domain  $\partial \mathcal{S}_t$  of SSPRK(3,3) (left figure, thin-line) and DP5 (right figure, thin-line).

## 4 Numerical Tests

In this section we consider two different scalar 1D hyperbolic conservation laws: the advection equation and Burgers' equation. We consider 1-periodic boundary conditions and different types of initial data. We numerically compute the approximate solution using the WENO5 spatial discretization combined with the different time-stepping schemes discussed above in order to verify the analytic results. Note that our analysis in Section 3 was based on linearizing the WENO5 scheme. Our calculations here use the fully nonlinear WENO5 procedure.

### 4.1 Advection Equation

We begin with the linear advection equation (1) with 1-periodic boundary conditions and two different choices of initial data

$$u^0(x) = f_1(x) = \sin(2\pi x), \quad \text{and} \quad u^0(x) = f_2(x) = \begin{cases} 1, & 0 \leq x \leq 0.25, \\ 0, & 0.25 < x < 1. \end{cases}$$

We use a uniform spatial grid with  $N = 100$  grid points ( $\Delta x = 0.01$ ) and discretize the PDE on this grid using the WENO5 discretization.

#### 4.1.1 First- and second-order time stepping

We first consider FE time stepping with the step size  $\Delta t = 50 \Delta x^5$  and compute the approximate solution until the final time  $T = 0.1$ . This requires approximately

Table 2: Linearly stable time step-sizes of different time-stepping schemes for the linear advection equation discretized in space with linearized WENO5.

Time stepping	Maximum time step-size	Function evaluations
FE	51.95 $\Delta x^5$	1
ERK2	1.73 $\Delta x^{5/3}$	2
Adams5	0.123 $\Delta x$	1
eBDF5	0.238 $\Delta x$	1
PC5	0.565 $\Delta x$	2
SSPRK(3,3)	1.43 $\Delta x$	3
DP5	1.79 $\Delta x$	6

$2 \times 10^7$  time steps. Figure 8 (left column) shows the numerical solutions and the exact solutions at the final time  $T = 0.1$  with different initial data, and Figure 8 (right column) shows the total variation of the numerical solutions as a function of time. Next, we use the midpoint ERK2 time stepping with

$$A = \begin{bmatrix} 0 & 0 \\ \frac{1}{2} & 0 \end{bmatrix}, \quad b = \begin{bmatrix} 0 \\ 1 \end{bmatrix}.$$

We take the step size  $\Delta t = \Delta x^{5/3}$  and compute the approximate solution until the final time  $T = 50.5$ . The numerical and exact solutions at the final time  $T = 50.5$  and the total variation of the numerical solutions as a function of time are shown in Figure 9. In this experiment we find that the FE and ERK2 time-stepping schemes are stable, when combined with WENO5 spatial discretization and a suitable time step-size. We remark that because of the very strict time-stepping restriction, the combination of either FE or ERK2 time stepping with WENO5 discretization may not be practical in real computations.

#### 4.1.2 Fifth-order time stepping

Because WENO5 is a fifth-order spatial discretization, it is natural to choose a time discretization which is fifth order as well. We now numerically study the fifth-order schemes listed above, i.e., Adams5, eBDF5, PC5, and DP5. Our examples select time step-sizes which satisfy the geometric stability condition, since otherwise numerical blow-up is observed. For example, Figure 10 shows the numerical solution at the time  $T = 0.05$  when Adams5 is employed with  $\Delta t = 0.13 \Delta x$ , that is with a CFL number just slightly larger than the geometric stability limit ( $\Delta t = 0.123 \Delta x$ ). We see that the numerical solution blows up early in the time integration. We emphasize that this instability occurs with the fully nonlinear WENO5. This indicates that our analysis (based on linearized WENO5) correctly predicts the linear stability bound of WENO5.

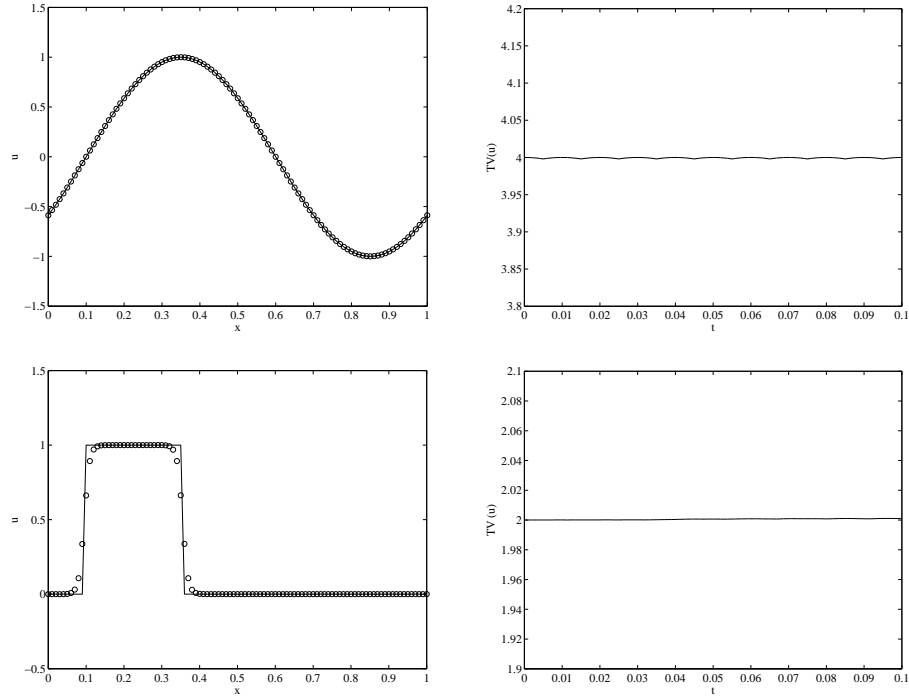


Figure 8: The left figures show the numerical and the exact solutions at the final time  $T = 0.1$  using FE time stepping for two different initial data. The right figures show the total variation of the numerical solutions as a function of time. The time step-size  $\Delta t = 50 \Delta x^5$  is chosen.

Note that our computations use the exact solution  $u(x, t) = u^0(x - t)$  to obtain the first four starting values for the multistep schemes. Similar results are observed when employing the SSPRK(3,3) method for the starting procedure.

We continue by considering  $\Delta t = 0.1 \Delta x$  and Adams5. This time step-size does not violate the geometric stability condition. Although the numerical solution is linearly stable and does not blow up, we observe tiny oscillations in the first few time steps (see Figure 11). These oscillations, which disappear quickly as time passes due to the dissipative property of WENO5 and the linear stability of the time integrators, may be a result of nonlinear instability. A similar behavior is observed for the other fifth-order time-stepping methods. By numerical experiment, we find that these tiny oscillations do not form if we choose the time step-sizes  $\Delta t \leq 0.02 \Delta x$ ,  $\Delta t \leq 0.20 \Delta x$ ,  $\Delta t \leq 0.20 \Delta x$  and  $\Delta t \leq 1.00 \Delta x$  for Adams5, eBDF5, PC5 and DP5, respectively. The numerical and exact solutions at the final time

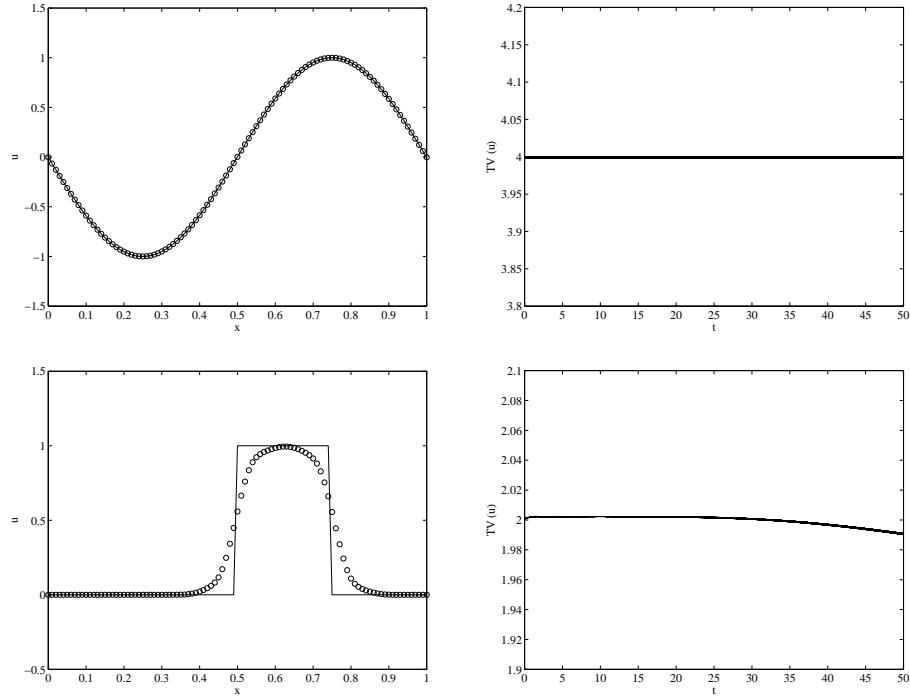


Figure 9: The left figures show the numerical solutions and the exact solutions at the final time  $T = 50.5$  using ERK2 time stepping for two different initial data. The right figures show the total variation of the numerical solutions as a function of time. The time step-size  $\Delta t = \Delta x^{5/3}$  is chosen.

$T = 50.5$  and the total variation of the numerical solutions as a function of time are shown in Figure 12 for eBDF5. The plots for Adams5, PC5 and DP5 are visually identical.

Among the three fifth-order ELM time-stepping methods (none of which have stability domains which include a part of imaginary axis  $[-i\beta, i\beta]$  with  $\beta > 0$ ) the eBDF5 scheme is the most efficient with respect to the avoidance of spurious oscillations.

A comparison of the performance of eBDF5 with that of DP5 (note that DP5 is a well-known fifth-order time-stepping method whose stability domain does include a part of the imaginary axis) is also interesting. We consider the initial condition  $u^0(x) = f_2(x)$  and use a uniform spatial grid with  $N = 200$  grid points. We choose the time step-size  $\Delta t = 0.2 \Delta x$  for eBDF5. Noting that the eBDF5 and DP5 methods require one and six function evaluations at each time step, respectively,

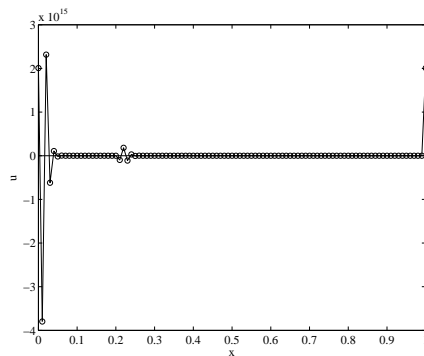


Figure 10: The numerical solution at the final time  $T = 0.5$  using Adams5 time stepping for the second initial data,  $f_2$ . The time step-size  $\Delta t = 0.13 \Delta x$  is chosen. The numerical solution blows up because the geometric stability condition is violated.

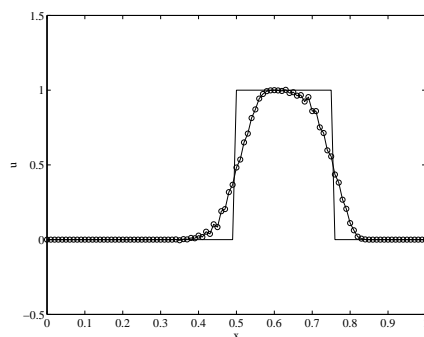


Figure 11: The numerical and exact solutions at the final time  $T = 0.5$  using Adams5 time stepping for the second initial data,  $f_2$ . The time step-size  $\Delta t = 0.1 \Delta x$  is chosen. The numerical solution is linearly stable, but tiny oscillations are present.

we choose the time step-size  $\Delta t = 1.2 \Delta x$  for DP5. Figure 13 compares the exact result against the numerical solutions obtained by these two time-stepping methods at time  $T = 0.02$ . The figure also gives the total variation of the numerical solutions as a function of time from  $t = 0$  to  $t = 2$ . The eBDF5 scheme is preferred for this example since the DP5 scheme produces small oscillations in the numerical solution. These oscillations occur at the beginning of the evolution and damp out as time passes. We note that this oscillatory behavior of the DP5 method can be eliminated

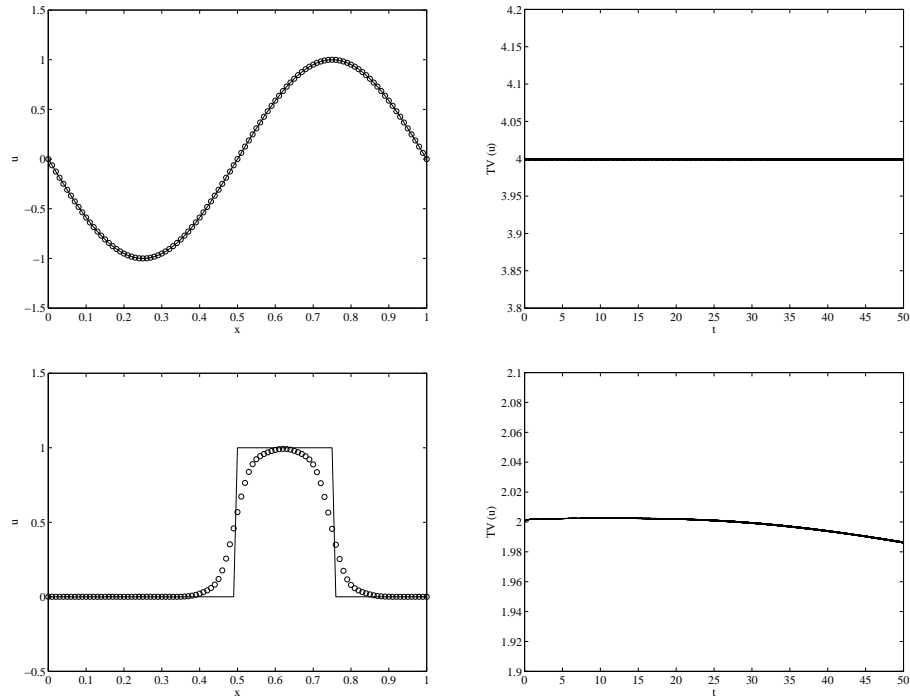


Figure 12: The left figures show the numerical solutions and the exact solutions at the final time  $T = 50.5$  using eBDF5 time stepping for two different initial data. The right figures show the total variation of the numerical solutions as a function of time. The time step-size  $\Delta t = 0.2 \Delta x$  is chosen.

by taking a smaller time step-size,  $\Delta t = \Delta x$ .

## 4.2 Burgers' Equation

As a second example, we consider the nonlinear Burgers' equation

$$u_t + \left( \frac{u^2}{2} \right)_x = 0, \quad x \in [0, 1], \quad t > 0,$$

with 1-periodic boundary conditions and the initial data  $u^0(x) = 2 + \sin(2\pi x)$ . As before, we select a uniform spatial grid with  $N = 100$  grid points and discretize the PDE on this grid using the WENO5 discretization.

For this problem the CFL number is  $\sigma = \frac{\Delta t}{\Delta x} \max |u(x, t)|$  and our choice of initial conditions dictates  $\max |u(x, t)| = 3$ . For each time-stepping method, we



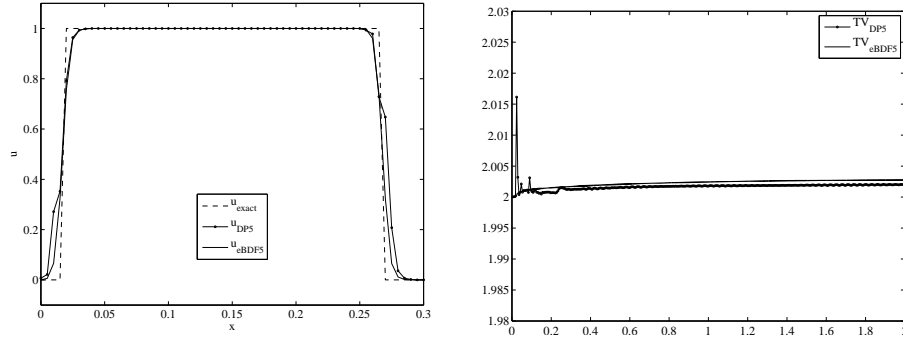


Figure 13: The left figure shows a zoomed view of the numerical solutions and the exact solutions at the final time  $T = 0.02$  using eBDF5 and DP5 time stepping. The right figure shows the total variation of the numerical solutions as a function of time from 0 to 2. The time step-sizes  $\Delta t = 0.2 \Delta x$  and  $\Delta t = 1.2 \Delta x$  are chosen for eBDF5 and DP5, respectively.

choose time step-sizes  $\Delta t \leq \sigma_g \Delta x / \max |u(x, t)|$ , based on the geometric stability limit on  $\sigma$ . We compare the numerical solutions arising from different methods with a reference solution obtained using a very fine grid.

Figure 14 shows the numerical and the reference solutions at the final time  $T = 0.1$  as well as the total variation of the numerical solution as a function of time. We begin by considering the FE time-stepping method with the step size  $\Delta t = (1/3) 50 \Delta x^5$ , just slightly smaller than the geometric stability limit. The results are numerically stable and free of oscillations. We remark that due to the severe time-step restriction we do not attempt to compute to  $T = 30.5$ , as is used in our other results below.

We next consider the midpoint ERK2 scheme with the time step-size  $\Delta t = (1/3) \Delta x^{5/3}$ . The numerical and the reference solutions at the final time  $T = 30.5$  as well as the total variation of the numerical solution as a function of time are provided in Figure 15. The results are stable and aside from a small initial jump, the total variation decreases with time.

A study for a selection of fifth-order schemes was also carried out. The numerical and the reference solutions at the final time  $T = 30.5$  along with the total variation of the numerical solutions are provided in Figure 16 for eBDF5 using the time step-size  $\Delta t = 0.05 \Delta x$ . The results are qualitatively similar to the ERK2 scheme. We further note that similar results were observed for the other fifth-order time integrators, i.e., Adams5, PC5 and DP5 using the step sizes  $\Delta t = 0.02 \Delta x$ ,  $\Delta t = 0.1 \Delta x$ , and  $\Delta t = 0.3 \Delta x$ , respectively.

As mentioned above, there is an initial jump in the total variation of the nu-

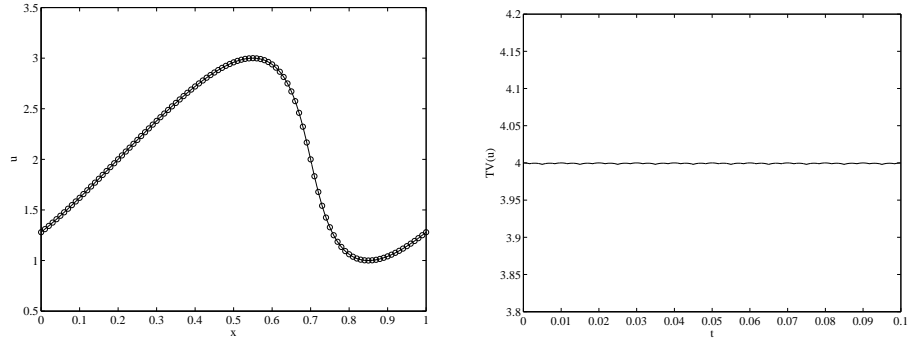


Figure 14: The left figure shows the numerical and the reference solutions at the final time  $T = 0.1$  using FE time stepping. The right figure shows the total variation of the numerical solution as a function of time. The time step-size  $\Delta t = (1/3) 50 \Delta x^5$  is chosen.

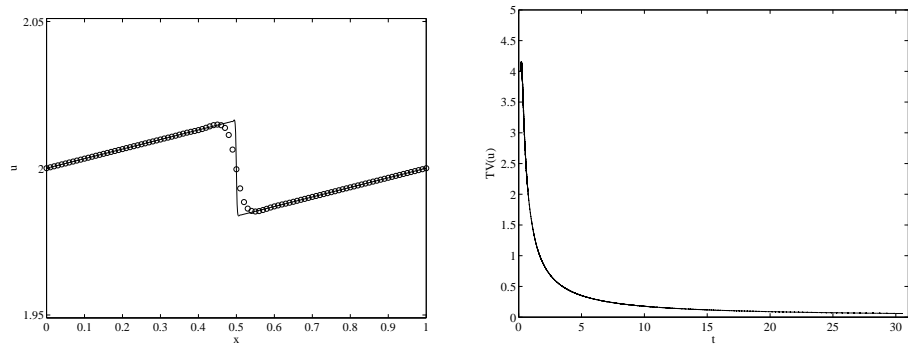


Figure 15: The left figure shows the numerical and the reference solutions at the final time  $T = 30.5$  using ERK2 time stepping. The right figure shows the total variation of the numerical solution as a function of time. The time step-size  $\Delta t = (1/3) \Delta x^{5/3}$  is chosen.

numerical solutions when the shock first forms at about  $T = 0.2$ . This jump arises for all the schemes we considered, including the SSP time-stepping schemes. See Figure 17 for results with the well-known SSPRK(3,3) scheme. Note that eBDF5 outperforms SSPRK(3,3) in this example: if we select  $\Delta t = 0.15 \Delta x$ , which corresponds to the computational work for the eBDF5 calculation in Figure 16, the solution gives severe oscillations.

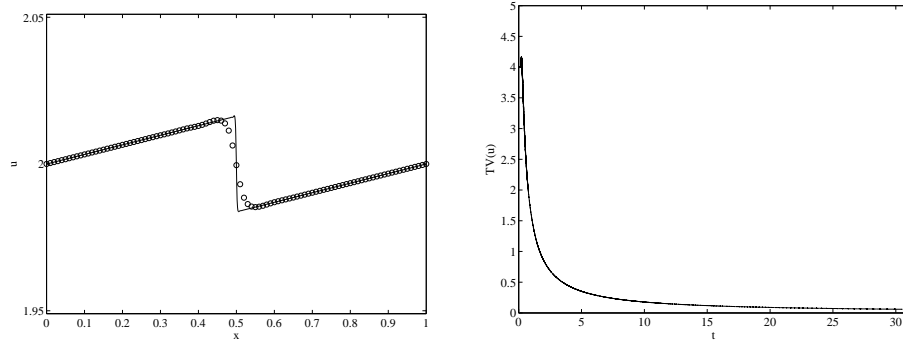


Figure 16: The left figure shows the numerical and the reference solutions at the final time  $T = 30.5$  using eBDF5 time stepping. The right figure shows the total variation of the numerical solution as a function of time. The time step-size  $\Delta t = 0.05 \Delta x$  is chosen.

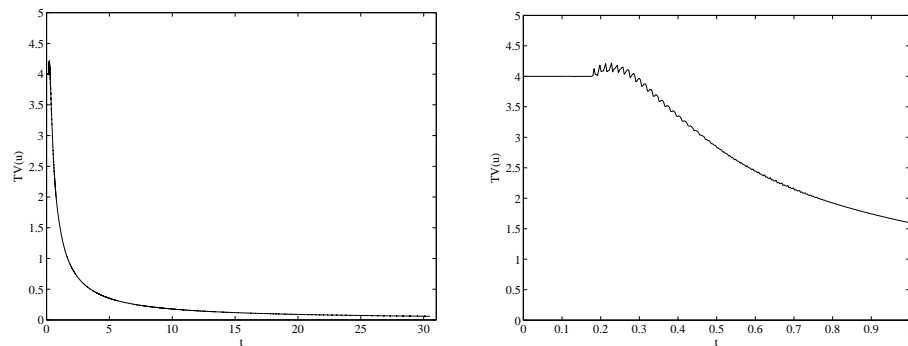


Figure 17: The left figure shows the total variation of the numerical solution as a function of time using SSPRK(3,3) time stepping. The right figure shows a zoomed view. The time step-size  $\Delta t = 0.1 \Delta x$  is chosen.

## 5 Conclusion

We have studied the linear stability of the WENO5 spatial discretization combined with explicit time-stepping schemes applied to the one-dimensional advection equation. Our main approach was a specialized linear stability analysis of the linear finite difference scheme resulting from freezing the nonlinear weights of the WENO5 method. Numerical tests then demonstrated that our results carry over to the fully nonlinear WENO5 case.

The main result is that it is not necessary for the stability domain of the time integrator to include a part of the imaginary axis. In particular, we have shown that the combination of WENO5 with the forward Euler and second-order Runge–Kutta methods is linearly stable provided very small time step-sizes are taken. In real computations, however, applying these two time integrators may not be practical because of the extremely strict time-stepping restrictions that they possess. We have further studied a variety of fifth-order multistep time discretizations whose stability domain does not include the imaginary axis but possess suitable linear stability properties when combined with WENO5. We have also shown that in practice these methods respect the TVD property of the solution in a similar way to strong stability preserving Runge–Kutta schemes; that is, they seem to have good nonlinear stability properties provided a suitably small time step is chosen.

A comparison between these multistep methods and high-order Runge–Kutta methods whose stability domain includes the imaginary axis has been presented. According to our analysis and numerical tests, the former class of methods (with no imaginary axis inclusion) may be competitive with the latter class (with imaginary axis inclusion), in terms of both accuracy and computational efficiency. We particularly recommend the eBDF5 scheme. The eBDF5 scheme has a mild time-stepping restriction and good monotonicity properties (see [16]) and gave the best performance of the fifth-order schemes we considered in our experiments.

## References

- [1] J. Blazek, (2001) *Computational fluid dynamics: principles and applications*, Elsevier, Oxford.
- [2] J. C. Butcher, (2008) *Numerical Methods for Ordinary Differential Equations*, Wiley.
- [3] S. Gottlieb and C.-W. Shu, (1998) *Total variation diminishing Runge-Kutta schemes*, Math. Comp. 67, 73–85.
- [4] S. Gottlieb and C.-W. Shu and E. Tadmor, (2001) *Strong stability-preserving high-order time discretization methods*, SIAM Rev. 43 (1), 89–112.
- [5] E. Hairer and G. Wanner, (1996) *Solving Ordinary Differential Equations II, Stiff and Differential-Algebraic Problems*, Springer.
- [6] A. Harten, (1983) *High resolution schemes for hyperbolic conservation laws*, J. Comput. Phys. 49, 357–393.
- [7] A. Harten and B. Engquist and S. Osher and S. Chakravarthy, (1987) *Uniformly high order accurate non-oscillatory schemes, III*, J. Comput. Phys. 71, 231–303.

- [8] A. Harten and S. Osher, (1987) *Uniformly high order accurate non-oscillatory schemes, I*, SIAM J. Numer. Anal. 24, 279–309.
- [9] C. Hirsch, (1988) *Numerical computation of internal & external flows: fundamentals of numerical discretization*, John Wiley & Sons, Inc., New York.
- [10] G.-S. Jiang and C.-W. Shu, (1996) *Efficient implementation of weighted ENO schemes*, J. Comput. Phys. 126 (1), 202–228.
- [11] D. I. Ketcheson and C. B. Macdonald and S. Gottlieb, (2009) *Optimal implicit strong stability preserving Runge–Kutta methods*, Appl. Numer. Math. 59 (2), 373–392.
- [12] C. B. Laney, (1998) *Computational gasdynamics*, Cambridge University Press, Cambridge.
- [13] D. Levy and E. Tadmor, (1998) *From semidiscrete to fully discrete: stability of Runge–Kutta schemes by the energy method*, SIAM Rev. 40 (1), 40–73.
- [14] X.-D. Liu and S. Osher and T. Chan, (1994) *Weighted essentially non-oscillatory schemes*, J. Comput. Phys. 115, 200–212.
- [15] S. Osher and S. Chakravarthy, (1984) *High resolution schemes and the entropy conditions*, SIAM J. Numer. Anal. 21, 955–984.
- [16] S. J. Ruuth and W. Hundsdorfer, (2005) *High-order linear multistep methods with general monotonicity and boundedness properties*, J. Comput. Phys. 209 (1), 226–248.
- [17] C.-W. Shu, (1987) *TVB uniformly high order schemes for conservation laws*, Math. Comp. 49, 105–121.
- [18] C.-W. Shu, (1988) *Total-variation-diminishing time discretizations*, SIAM J. Sci. Statist. 9, 1073–1084.
- [19] C.-W. Shu, (1997) *Essentially Non-Oscillatory and Weighted Essentially Non-Oscillatory Schemes for Hyperbolic Conservation Laws*, Brown University, ICASE Report, pp. 97-65, Prepared for NASA Langley Research Center.
- [20] C.-W. Shu and S. Osher, (1988) *Efficient implementation of essentially non-oscillatory shock-capturing schemes*, J. Comput. Phys. 77, 439–471.
- [21] R. Wang and R. J. Spiteri, (2007) *Linear instability of the fifth-order WENO method*, SIAM J. Numer. Anal. 45 (5), 1871–1901.



## RECENT REPORTS

18/10	A Mathematical Model of Tumor-Immune Interactions	Robertson-Tessi El-Kareh Goriely
19/10	Elastic cavitation, tube hollowing, and differential growth in plants and biological tissues	Goriely Moulton Vandiver
20/10	Asymptotic expressions for the nearest and furthest dislocations in a pile-up against a grain boundary	Hall
21/10	Cardiac electromechanics: the effect of contraction model on the mathematical problem and accuracy of the numerical scheme	Pathmanathan Chapman Gavaghan Whiteley
22/10	Fat vs. thin threading approach on GPUs: application to stochastic simulation of chemical reactions	Klingbeil Erban Giles Maini
23/10	Asymptotic analysis of a system of algebraic equations arising in dislocation theory	Hall Chapman Ockendon
25/10	Preconditioning for Allen-Cahn Variational Inequalities with Non-Local Constraints	Blank Sarbu Stoll
26/10	On an evolution equation for sand dunes	Ellis Fowler
27/10	On Liquid Films on an Inclined Plate	Benilov Chapman McLoed Ockendon Zubkov
28/10	An a posteriori error analysis of a mixed finite element Galerkin approximation to second order linear parabolic problems	Memon Nataraj Pani
29/10	A Priori Error Estimates for Semidiscrete Finite Element Approximations to Equations of Motion Arising in Oldroyd Fluids of Order One	Goswami Pani
30/10	The Landau-de Gennes theory of nematic liquid crystals: Uniaxiality versus Biaxiality	Majumdar
31/10	The Radial-Hedgehog Solution in Landau-de Gennes' theory	Majumdar
32/10	Nonlinear instability in flagellar dynamics: a novel modulation mechanism in sperm migration?	Gadelha Gaffney Smith Kirkman-Brown
33/10	Error bounds on block GaussSeidel solutions of coupled multi-physics problem	Whiteley Gillow Tavener

34/10	A random projection method for sharp phase boundaries in lattice Boltzmann simulations	Reis Dellar
35/10	Regularized Particle Filter with Langevin Resampling Step	Duan Farmer Moroz
36/10	Sequential Inverse Problems Bayesian Principles and the Logistic Map Example	Duan Farmer Moroz
37/10	Circumferential buckling instability of a growing cylindrical tube	Moulton Goriely
38/10	Preconditioners for state constrained optimal control problems with Moreau-Yosida penalty function	Stoll Wathen
39/10	Local synaptic signaling enhances the stochastic transport of motor-driven cargo in neurons	Newby Bressloff
40/10	Convection and Heat Transfer in Layered Sloping Warm-Water Aquifer	McKibbin Hale Style
41/10	Optimal Error Estimates of a Mixed Finite Element Method for Parabolic Integro-Differential Equations with Non Smooth Initial Data	Goswami Pani Yadav

**Copies of these, and any other OCCAM reports can be obtained from:**

**Oxford Centre for Collaborative Applied Mathematics  
Mathematical Institute  
24 - 29 St Giles'  
Oxford  
OX1 3LB  
England**

**[www.maths.ox.ac.uk/occam](http://www.maths.ox.ac.uk/occam)**